中國機械工程學刊第四十六卷第三期第 287~296 頁(民國一百一十四年)
Journal of the Chinese Society of Mechanical Engineers, Vol.46, No.3, pp 287~296 (2025)

Optimal Design to Reduce the Vibration of Omnidirectional Three Wheeled Mobile Robot

Khoa Viet Nguyen[*,***] and Ngoc Van Bach Pham[**,***]

Key words: Mobile robot, Omnidirectional three wheeled, Vibration, Absorber.

Abstract

Recent image-based robotic systems use image identification to control robots in many industry fields. When the robot moves on an uneven ground the view of camera attached to the robot will be changed over time, and together with the effect of robot vibration the images will be blurred. Thus, the elimination of vibration of the mobile robot is very important for image processing with high accuracy. This paper presents the optimal design of an omnidirectional wheeled mobile robot (OMR) to reduce its vibration. The formulas for calculating the vibration of the triangular OMR equipped with vibration absorber systems moving on an unevenness ground is established. The relationship between the vibration amplitude and parameters of the OMR is investigated to determine optimal parameters to reduce the robot vibration. The experiment has also been carried out to verify the proposed design of the OMR.

Introduction

Mobile robots have been playing an important role in many fields such as national defense, military operations, interstellar exploration, environments, and social services. Based on the applications, different kinds of mobile robots have been designed. For example, one kind of mobile robot is wheeled mobile platforms with mounted manipulators (Kim et al., 2010), another kind is the image-based control robot. In general, these robots are restricted to move on even ground, however they are flexible and robust. For instance, a wheeled mobile platform has been developed for the two-arm humanoid McBot robot (Ma et al., 2008) with a high performance of mobility. Several systems have been designed over the last decades (Bischoff et al., 1997; Connette et al., 2008) with the main difference in the type and number of wheels (Muir et al., 1986; Campion et al., 1996). Conventional wheeled mobile robot (WMR) is restricted in their motion because they cannot move sideways without a preliminary maneuvering. Therefore, many mechanisms have been designed to improve the maneuverability of WMR. However, the problem of non-holonomic system in the conventional WMR cannot be solved since it cannot drive in all possible direction. Thus, this robot is called 'non-holonomic'. Meanwhile, a holonomic robot using omnidirectional wheels, can be driven in any direction. In the last decade, Swedish wheel has emerged as a great improvement for mobile robotics and has attracted many researchers in the field of OMR (Ashmore et al., 2002; Baede, 2006; Liu et al., 2003; Taheri et al., 2020). Therefore, the OMR are now very popular due to their low cost, simplicity, and their power in navigation that can be used for many applications in various environments. In general, the omnidirectional wheels discontinuously contact the floor (i.e. universal wheels and Mecanum wheels) leading to the problem of vibration. The more wheels are applied, the less vibration problem will be obtained. However, the design of robot with more wheels will be more complex and it needs the suspensions to the wheels contacted to the ground, which is a very difficult task especially on uneven floors.

Nowadays, image-based control robots have been widely studied. The image-based robotic systems use predicted future state images to control robots (Foo et al., 2005; Kumar et al., 2018). Therefore, the accuracy of the prediction of the future state image affects the performance of the robot. In order to predict images, current studies assume that the camera captures the entire scene and that the environment is static (Ishihara et al., 2022), but these assumptions are not always met in practice, thus many efforts have been devoted to develop robust image prediction systems (Pathak et al., 2018; Finn et al., 2016; Ebert et al., 2017; Wu et al., 2019; Hirose et al., 2019; Hirose et al., 2019).

For mobile robot, since a camera is attached to the robot, its view will change over time, and in addition due to the effect of vibration of robot during its

Paper Received March, 2024. Revised November, 2024. Accepted December, 2024. Author for Correspondence: Ngoc Van Bach Pham

[*] *Department of Structural Health Monitoring, Institute of Mechanics, Vietnam Academy of Science and Technology, Ha Noi, Vietnam*

*** *Department of Sefas, Vietnam National Space Center, Vietnam Academy of Science and Technology, Ha Noi, Vietnam*

****VNU University of Engineering and Technology, Vietnam National University, Hanoi*

movement, the images will be blurred. As mentioned above, the usage of more wheels needs the more complex design, so the image-based mobile robots in general have a small number of wheels leading to vibration problems. Therefore, the elimination of vibration of mobile robot is very important to improve the accuracy of the image prediction. There are various studies concern the vibration of mobile robots or mobile vehicles presented in literature. To control the vibration of mobile robots, the passive, semi-passive and active suspension systems have been applied. Naderi et al. (2001) presented the kinematic and dynamic modeling of a two degrees of freedom manipulator attached to a vehicle. The influence of the dynamic interaction between the vehicle and the manipulator is significant. Mrad et al. (1999) studied the use the dynamic vibration absorber for vibration control of mobile robot vehicle. Matsuhisa et al. (1995) presented a method for vibration control of a rope wave carrier using passive dynamic vibration absorbers. Zhong et al. (2012) proposed approaches based on particle swarm optimization for problems of vibration reduction of suspended mobile robot with a manipulator. Nagai (1993) presented researches on active suspensions for ground vehicles. Liu et al. (2005) used the semi-active fuzzy sliding mode control of full vehicle and suspensions to control the vibration of a vehicle. Lin et al. (2023) presented an automatic calibration of Tool Center Point for six degree of freedom robot using a laser sensor to process runout, and offsets calibration after installing the tool. In industrial robotic systems, the nonlinear vibration behavior may occur under some specific conditions leading to chattering and uneven product quality. Thus, the nonlinear behavior of robot systems should be considered. Felix et al. (2014) presented methods for controlling the nonlinear dynamics and chaos behavior of a robotic arm using the nonlinear saturation control and the optimal linear feedback control. Razzaghi et al. (2019) studied the nonlinear dynamics and control of a jumper robot based on the inertial actuation concept that can navigate in three-dimensional environments. Recently, Wang et al. (2021) presented a method for the identification and prediction of nonlinear behavior in a robotic arm system based on machine learning. As a result, a highly accurate prediction and identification model system for nonlinear and chaotic motion in robotic arms is obtained. However, since the size of robot in this study is small and the speed of robot is slow, then the nonlinear behavior of the robot is not a scope of this paper.

Although many types of mobile robots have been developed for image-based mobile robotic systems, most them have focused on algorithms for the image processing. While, the vibration elimination for the image-based control mobile robot has not been played an important role. Especially, the optimal design for the OMR to reduce the vibration has not been addressed.

This work aims to present a new design of a triangular OMR equipped with three wheels and three vibration absorber systems to reduce the vibration of the camera attached on the robot. The novelty of this paper lies in the following: 1) The formulas for calculating the vibration of the triangular OMR moving on an unevenness ground are established. 2) The formula for calculating the mass moments of inertia of the triangular robot body based on the shape of the robot are presented. 3) The derived formulas are applied to calculate the optimal parameters of the robot such as velocity, stiffness of springs, damping coefficients, to reduce its vibration when it moves on different uneven surfaces. In this paper, numerical simulations are conducted and provided. Experiments have been carried out to justify the efficiency of the proposed method. The proposed method has an advantage that the absorber systems are simple, while the numerical simulation and experiment results show that the optimal design of robot is very effective to reduce the vibration of the robot.

Theoretical background

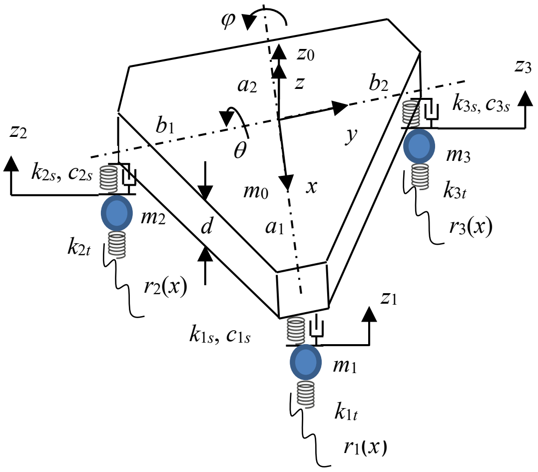

Fig. 1. Model of the OMR

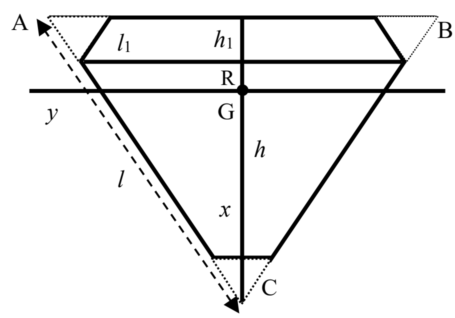

Fig. 2. The top-view of the robot body

In this study, the model of OMR is considered as presented in Figure. 1. Each wheel is modeled as a mass of m and a spring k_t. In order to reduce the vibration of the robot body, three suspension systems assembled by springs k_{1s}, k_{2s}, k_{3s} and dampers c_{1s}, c_{2s}, c_{3s} are equipped with the OMR at three wheels. The coordinate origin is located at the gravitational central. In this study, we assume that: the OMR moves along the x-axis with a constant velocity v; the robot body has 6 degrees of freedom: the translation z_1 of the center of gravity of robot body, the translations z_1, z_2, z_3 of three wheels, rotations θ and φ about the x-axis and y-axis.

The uneven functions of the ground at three wheels are assumed to be expressed as:

$$\begin{aligned} r_1(x) &= \frac{\overline{d}_1}{2}\cos\left(\frac{2\pi x}{\overline{l}_1}+\theta_1\right) = \frac{\overline{d}_1}{2}\cos\left(\frac{2\pi vt}{\overline{l}_1}+\theta_1\right) \\ r_2(x) &= \frac{\overline{d}_2}{2}\cos\left(\frac{2\pi x}{\overline{l}_2}+\theta_2\right) = \frac{\overline{d}_2}{2}\cos\left(\frac{2\pi vt}{\overline{l}_2}+\theta_2\right) \\ r_3(x) &= \frac{\overline{d}_3}{2}\cos\left(\frac{2\pi x}{\overline{l}_3}+\theta_3\right) = \frac{\overline{d}_3}{2}\cos\left(\frac{2\pi vt}{\overline{l}_3}+\theta_3\right) \end{aligned} \tag{1}$$

Here: $\overline{d}_1$, $\overline{d}_2$, $\overline{d}_3$ $\overline{l}_1$, $\overline{l}_2$, $\overline{l}_3$ are the depths and lengths of the unevenness of the ground at wheel 1, wheel 2, and wheel 3, respectively; θ_1, θ_2, θ_3 present the different phase angles between the wheel 1, wheel 2, and wheel 3, respectively.

In order to derive the governing equation of motion of the OMR, the mass moments of inertia I_x, I_y of robot body need to be calculated. From the geometry of the robot body as shown in Fig. 2, the mass moments of inertia I_x, I_y of robot body can be calculated as the following formulas:

$$\begin{aligned} I_y &= 2\rho d\left(\begin{aligned} &\int_{h_1-R}^{h-h_1-R}\int_0^{-\frac{l}{2h}x+\frac{l(h-R)}{2h}} x^2 dydx \\ &+\int_{-R}^{h_1-R}\int_0^{\frac{l_1}{2h_1}x+\frac{l}{2}+\frac{l_1(h-2h_1)}{2h_1}} x^2 dydx \end{aligned}\right) \\ &= 2\rho d\left(\begin{aligned} &-\frac{2lh_1^3R}{3h}+\frac{lh_1^3}{3}-\frac{lh_1^2h}{4}+\frac{lh_1^2R}{2}+\frac{lh^3}{24}-\frac{lh^2R}{6} \\ &+\frac{lhR^2}{4}-\frac{5h_1^3l_1}{24}+\frac{2h_1^2l_1R}{3}-\frac{3h_1l_1R^2}{4} \end{aligned}\right) \end{aligned} \tag{2}$$

$$\begin{aligned} I_x &= 2\rho d\left(\begin{aligned} &\int_{h_1-R}^{h-h_1-R}\int_0^{-\frac{l}{2h}x+\frac{l(h-R)}{2h}} y^2 dydx \\ &+\int_{-R}^{h_1-R}\int_0^{\frac{l_1}{2h_1}x+\frac{l}{2}+\frac{l_1(h-2h_1)}{2h_1}} y^2 dydx \end{aligned}\right) \\ &= 2\rho d\left(\begin{aligned} &-\frac{l^3h_1^3}{24h^2}+\frac{l^3h_1^2}{16h}+\frac{l^3h}{96}-\frac{3l^2h_1a_1}{16} \\ &+\frac{7lh_1a_1^2}{24}-\frac{5h_1l_1^3}{32} \end{aligned}\right) \end{aligned} \tag{3}$$

where ρ and d are the mass density and the thickness of the robot body, respectively; h, l are the height and the side of the triangle ABC, respectively. G is the centroid of the robot body.

The kinetic energy of the robot system can be calculated as the following formula:

$$T = \frac{1}{2}m_0\dot{z}_0^2 + \frac{1}{2}I_x\dot{\varphi}^2 + \frac{1}{2}I_y\dot{\theta}^2 \frac{1}{2}m_1\dot{z}_1^2 + \frac{1}{2}m_2\dot{z}_2^2 + \frac{1}{2}m_3\dot{z}_3^2 \tag{4}$$

where z_0, z_1, z_2, z_3 are displacements in the z direction of the robot body and the three wheels.

The potential energy of the robot can be expressed as:

$$\begin{aligned} \Pi &= \frac{1}{2}k_t\left(z_1-r_1\right)^2 + \frac{1}{2}k_t\left(z_2-r_2\right)^2 + \frac{1}{2}k_t\left(z_3-r_3\right)^2 \\ &+\frac{1}{2}k_{1s}\left(z_0-z_1-a_1\theta\right)^2 + \frac{1}{2}k_{2s}\left(z_0-z_2+a_2\theta+b_1\varphi\right)^2 \\ &+\frac{1}{2}k_{3s}\left(z_0-z_3+a_2\theta-b_2\varphi\right)^2 \end{aligned} \tag{5}$$

where ϕ and θ are rotational angles about the x and y axes, respectively.

The dissipation function is calculated by the following formula:

$$\begin{aligned} D &= \frac{1}{2}c_{1s}\left(\dot{z}_0-\dot{z}_1-l_1\theta\right)^2 + \frac{1}{2}c_{2s}\left(\dot{z}_0-\dot{z}_2+l_2\dot{\theta}+b_1\dot{\varphi}\right)^2 \\ &+\frac{1}{2}c_{3s}\left(\dot{z}_0-\dot{z}_3+a_2\dot{\theta}-b_2\dot{\varphi}\right)^2 \end{aligned} \tag{6}$$

where b_1, b_2, l_1, l_2 are the distances from wheels 2 and 3 to the x-axis, and from wheels 1 and 2 to the y-axis, respectively.

In order to derive the governing equation of motion of the robot, Lagrange method is applied (Jazar et al., 2008):

$$\frac{d}{dt}\left(\frac{\partial T}{\partial \dot{w}_r}\right) - \frac{\partial T}{\partial w_r} + \frac{\partial D}{\partial \dot{w}_r} + \frac{\partial \Pi}{\partial w_r} = f_r \tag{7}$$

where w_r, r=1,2,..,6 are generalized coordinates: $w_1=z_0$, $w_2=z_1$, $w_3=z_2$, $w_4=z_3$, $w_5=\theta$, $w_6=\varphi$; f_r, r=1, 2,..,6 are nonconservative generalized forces associated to w_r. In this problem $\frac{\partial T}{\partial w_r}=0$ and nonconservative forces are zero, thus Equation (7) can be rewritten as:

$$\frac{d}{dt}\left(\frac{\partial T}{\partial \dot{w}_r}\right) + \frac{\partial \Pi}{\partial w_r} + \frac{\partial D}{\partial \dot{w}_r} = 0. \tag{8}$$

Applying Lagrange method, the following equations are derived:

$$\begin{aligned} &m_0\ddot{z}_0 + c_{1s}\left(\dot{z}_0-\dot{z}_1-a_1\dot{\theta}\right) + c_{2s}\left(\dot{z}_0-\dot{z}_2+a_2\dot{\theta}+b_1\dot{\varphi}\right) \\ &+c_{3s}\left(\dot{z}_0-\dot{z}_3+a_2\dot{\theta}-b_2\dot{\varphi}\right) \\ &+k_{1s}\left(z_0-z_1+a_1\theta\right) + k_{2s}\left(z_0-z_2+a_2\theta+b_1\varphi\right) \\ &+k_{3s}\left(z_0-z_3+a_2\theta-b_2\varphi\right) = 0 \end{aligned} \tag{9}$$

$$\begin{aligned} &I_x\ddot{\varphi} + c_{2s}b_1\left(\dot{z}_0-\dot{z}_2+a_2\dot{\theta}+b_1\dot{\varphi}\right) - c_{3s}b_2\left(\dot{z}_0-\dot{z}_3+a_2\dot{\theta}-b_2\dot{\varphi}\right) \\ &+k_{2s}b_1\left(z_0-z_2-a_2\theta+b_1\varphi\right) - k_{3s}b_2\left(z_0-z_3+a_2\theta-b_2\varphi\right) = 0 \end{aligned} \tag{10}$$

$$\begin{aligned} &I_y\ddot{\theta} - c_{1s}a_1\left(\dot{z}_0-\dot{z}_1-a_1\dot{\theta}\right) + c_{2s}a_2\left(\dot{z}_0-\dot{z}_2+a_2\dot{\theta}+b_1\dot{\varphi}\right) \\ &+c_{3s}a_2\left(\dot{z}_0-\dot{z}_3+a_2\dot{\theta}-b_2\dot{\varphi}\right) \\ &-k_{1s}a_1\left(z_0-z_1-a_1\theta\right) + k_{2s}a_2\left(z_0-z_2+a_2\theta+b_1\varphi\right) \\ &+k_{3s}a_2\left(z_0-z_2+a_2\theta-b_2\varphi\right) = 0 \end{aligned} \tag{11}$$

$$\begin{aligned} &m_1\ddot{z}_1 - c_{1s}\left(\dot{z}_0-\dot{z}_1-a_1\dot{\theta}\right) + k_tz_1 - k_{1s}\left(z_0-z_1+a_1\theta\right) \\ &= k_tr_1. \end{aligned} \tag{12}$$

$$m_2\ddot{z}_2 - c_{2s}\left(\dot{z}_0 - \dot{z}_2 + a_2\dot{\theta} + b_1\dot{\varphi}\right) + k_t z_2 - k_{2s}\left(z_0 - z_2 + a_2\theta + b_1\varphi\right) = k_t r_2 \tag{13}$$

$$m_3\ddot{z}_3 - c_{3s}\left(\dot{z}_0 - \dot{z}_3 + a_2\dot{\theta} - b_2\dot{\varphi}\right) + k_t z_3 - k_{3s}\left(z_0 - z_3 + a_2\theta - b_2\varphi\right) = k_t r_3 \tag{14}$$

If we let:

$$\mathbf{M} = \begin{bmatrix} m_0 & & & & & \\ & I_x & & 0 & & \\ & & I_y & & & \\ & & & m_1 & & \\ & 0 & & & m_2 & \\ & & & & & m_3 \end{bmatrix}, \mathbf{F} = \begin{bmatrix} 0 \\ 0 \\ 0 \\ k_t r_1 \\ k_t r_2 \\ k_t r_3 \end{bmatrix}, \mathbf{D} = \begin{bmatrix} m_0 \\ I_x \\ I_y \\ m_1 \\ m_2 \\ m_3 \end{bmatrix} \tag{15}$$

$$\mathbf{K} = \begin{bmatrix} k_{11} & k_{12} & k_{13} & -k_{1s} & -k_{2s} & -k_{3s} \\ k_{21} & k_{22} & k_{23} & 0 & -k_{2s}b_1 & -k_{3s}b_2 \\ k_{31} & k_{32} & k_{33} & k_{1s}a_1 & -k_{2s}a_2 & -k_{3s}a_2 \\ -k_{1s} & 0 & k_{1s}a_1 & m_1 & 0 & 0 \\ -k_{2s} & -k_{2s}b_1 & -k_{2s}a_2 & 0 & m_2 & 0 \\ -k_{3s} & -k_{3s}b_2 & -k_{3s}a_2 & 0 & 0 & m_3 \end{bmatrix} \tag{16}$$

$$\mathbf{C} = \begin{bmatrix} c_{11} & c_{12} & c_{13} & -c_{1s} & -c_{2s} & -c_{3s} \\ c_{21} & c_{22} & c_{23} & 0 & -c_{2s}b_1 & c_{3s}b_2 \\ c_{31} & c_{32} & c_{33} & c_{1s}a_1 & -c_{2s}a_2 & -c_{3s}a_2 \\ -c_{1s} & 0 & c_{1s}a_1 & c_{1s} & 0 & 0 \\ -c_{2s} & -c_{2s}b_1 & -c_{2s}a_2 & 0 & -c_{2s} & 0 \\ -c_{3s} & c_{3s}b_2 & -c_{3s}a_2 & 0 & 0 & c_{3s} \end{bmatrix} \tag{17}$$

where the components of matrices **K** and **C** are calculated as

$$\begin{aligned} &k_{11} = k_{1s} + k_{2s} + k_{3s},\ k_{12} = k_{2s}b_1 - k_{3s}b_2 \\ &k_{13} = -k_{1s}a_1 + k_{2s}a_2 + k_{3s}a_2,\ k_{21} = k_{12} \\ &k_{22} = k_{2s}b_1^2 - k_{3s}b_2^2,\ k_{23} = k_{2s}b_1a_2 - k_{3s}b_2a_2 \\ &k_{31} = k_{13},\ k_{32} = k_{23},\ k_{33} = k_{1s}a_1^2 + k_{2s}a_2^2 + k_{3s}a_2^2 \end{aligned} \tag{18}$$

$$\begin{aligned} &c_{11} = c_{1s} + c_{2s} + c_{3s},\ c_{12} = c_{2s}b_1 - c_{3s}b_2 \\ &c_{13} = -c_{1s}a_1 + c_{2s}a_2 + c_{3s}a_2,\ c_{21} = c_{12} \\ &c_{22} = c_{2s}b_1^2 - c_{3s}b_2^2,\ c_{23} = c_{2s}b_1a_2 - c_{3s}b_2a_2 \\ &c_{31} = c_{13},\ c_{32} = c_{23},\ c_{33} = c_{1s}a_1^2 + c_{2s}a_2^2 + c_{3s}a_2^2 \end{aligned} \tag{19}$$

then the governing vibration equation of the robot will be expressed in the matrix form as follows:

$$\mathbf{M}\ddot{\mathbf{D}} + \mathbf{C}\dot{\mathbf{D}} + \mathbf{K}\mathbf{D} = \mathbf{F}\,. \tag{20}$$

Solving this equation using Newmark algorism, the dynamic responses of the mobile robot will be obtained.

Numerical simulation

Numerical simulations for an OMR with three wheels are conducted. The body of robot is made by aluminum. Parameters of the robot body are: The mass density is 2702 kg/m^3; the thickness and the side of robot body d=0.006m and l=0.3464 m, respectively; The stiffness of springs $k_{1s} = k_{2s} = k_{3s}$ and damping coefficients $c_{1s} = c_{2s} = c_{3s}$. The depth of unevenness $\overline{l}$ ranging from 0.05 m to 0.1 m are applied. For our purpose, the optimal parameters will be designed for the robot body m_0=10 kg, the wheel mass m=2.5/3 kg, and the velocity is up to 0.5 m/s. The camera will be placed at the center of gravity of the robot body to minimize the influence of rotations on the camera signal, thus the translation of the robot will be investigated to find the optimal parameters for minimizing the robot vibration. The maximum displacement-time history of the OMR will be calculated to investigate the influence of the design parameters: velocity, stiffness of springs, damping coefficients on the vibration of the robot to choose the optimal parameters.

Numerical simulations show that if the spring constant is too high, the camera will be subjected to a very rough vibration under high-frequency disturbances leading to blur captured images. Therefore, in this paper, the investigation of the spring constant in the range only from 0 to 2000 N/m will be presented. However, it should be noted that if the spring constant is too low, the natural frequency of the robot will be low, and thus the heave, rolling, and pitching will be large. This will be an important notation to choose the suitable spring constant.

Influence of the velocity and spring constant on the vibration of robot

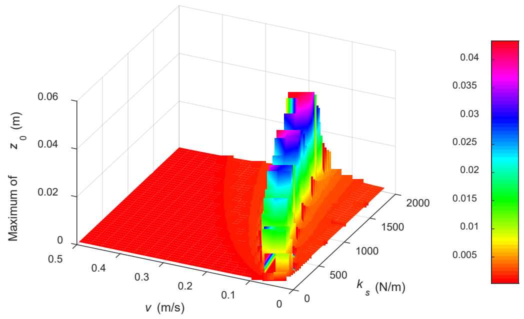

a) $\overline{l}$ =0.05 m

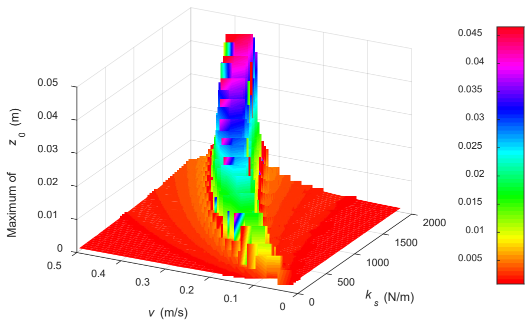

b) $\overline{l}$ =0.1 m

Fig. 3. Maximum displacement of the robot body versus k_s and v

In order to study the simultaneous influence of the velocity and spring constant on the vibration of robot, the maximum displacement of the robot body moving on the ground in duration of 4s with different velocities, and different spring constant is calculated. The influence of damping coefficient will be investigated in the next section, thus in this section it is fixed at c_s =0. Figure 3 presents the maximum displacement of the robot body versus v and k_s when $\overline{l}$ = 0.05 m, 0.1 m. As shown in Fig. 3a, when $\overline{l}$ = 0.05 m spring constant smaller than 2000 N/m can be applied to avoid the high vibration of the robot with the velocity ranging from 0.25 m/s to 0.5 m/s. However, when $\overline{l}$ = 0.1 m, the spring constant and velocity should be chosen appropriately to avoid the high vibration of robot as shown in Fig. 3b. For example, if the velocity is 0.2 m/s the spring constant should be higher than 700 N/m and if the velocity is 0.4 m/s the spring constant should be smaller than 1200 N/m.

Influence of the damping coefficient and spring constant on the vibration of robot

Fig. 4 shows the relationship between the maximum displacement of the robot body and the damping c_s and spring constant k_s with different lengths of unevenness $\overline{l}$. When both the length of unevenness and velocity are small: $\overline{l}$ = 0.05 m and v=0.25 m/s, the maximum displacement of robot body increases when c_s and k_s increase as shown in Figs. 4a, 4b. Thus, to reduce the vibration of robot, c_s and k_s should be small. When the length unevenness increases $\overline{l}$ = 0.1 m but the velocity is small v=0.25 m/s, the maximum displacement of robot body is significant when c_s is smaller than 50 Ns/m and k_s ranges from 500 N/m to 1100 N/m as shown in Fig. 4c. From this figure, to reduce the vibration of robot, we can use springs with $k_s \le 2000$ N/m and dampers with $c_s \ge 50$ Ns/m or we can use dampers with $c_s \le 2000$ N/m and springs with k_s outside the range from 500 N/m to 1100 N/m. When both the length of unevenness and velocity are high: $\overline{l}$ = 0.1 m and velocity v=0.5 m/s, the damping coefficient c_s and spring constant k_s should be small to reduce the vibration of robot as shown in Fig. 4d.

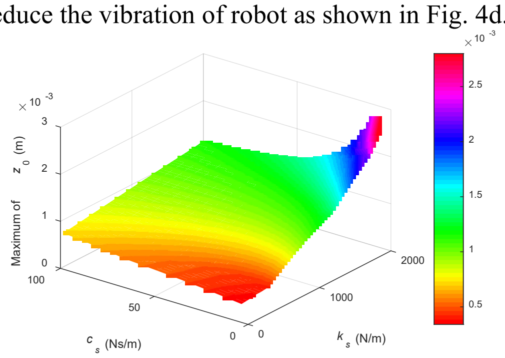

a) $\overline{l}$ =0.05 m, v=0.25m/s

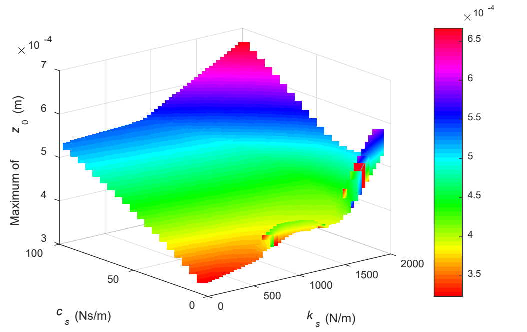

b) $\overline{l}$ =0.05 m, v=0.5m/s

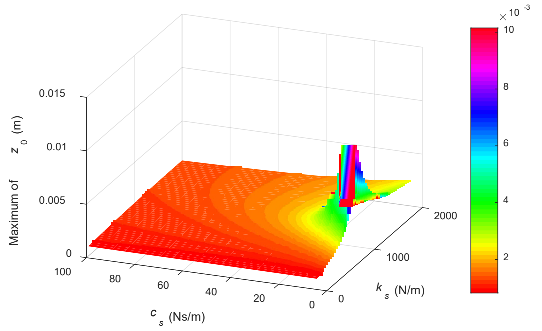

c) $\overline{l}$ =0.1 m, v=0.25m/s

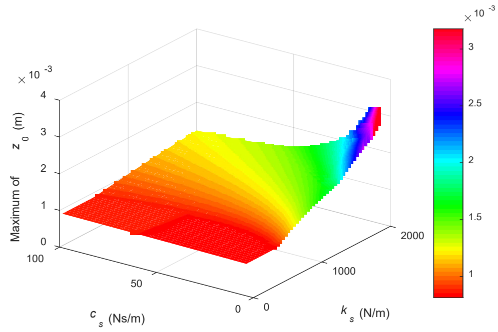

d) $\overline{l}$ =0.1 m, v=0.5m/s

Fig. 4. Maximum displacement of the robot body versus c_s and k_s

Influence of the length of unevenness and the spring constant on the vibration of robot

Fig. 5 shows the maximum displacement of the robot body versus $\overline{l}$ and k_s when v=0.25 m/s, 0.5 m/s. As can be observed from this figure, the spring constant should be chosen appropriately with the length of unevenness of the ground and the velocity. For example, when $\overline{l}$ = 0.8 m and v=0.25 m/s, the spring constant should be smaller than 800 N/m, but when $\overline{l}$ = 0.1 m, the spring constant should be greater than 1200 N/m to reduce the vibration of robot.

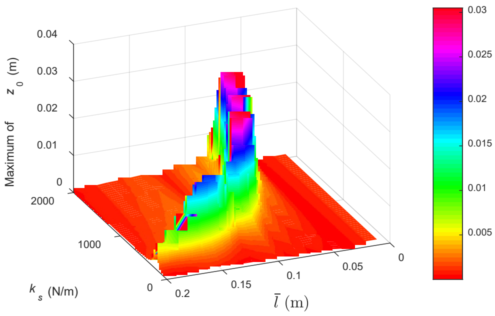

a) v=0.25m/s

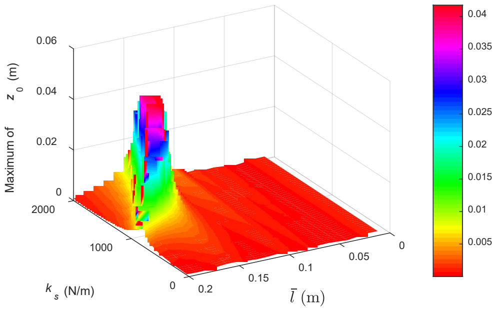

b) v=0.5m/s

Fig. 5. Maximum displacement of the robot body versus $\bar{l}$ and k_s

Influence of the unevenness and the velocity on the vibration of robot

Finally, let us investigate the simultaneous influence of the level of unevenness and the velocity on the vibration of robot. As can be seen from Eq. (20), the depth of unevenness $\bar{d}$ corresponds to the amplitude of excitation force, thus it can be considered as a proportional factor for the vibration amplitude of robot under the excitation force. As a result, the depth of unevenness influences only the vibration amplitude of the robot. To demonstrate this, two different levels of the depth of unevenness $\bar{d}$ =0.001 m and $\bar{d}$ =0.002 m are applied. As can be observed from Fig. 6a and 6b, the graphs of vibration of the robot in these two cases are similar, but their amplitudes are proportional to each other. Therefore, in this paper the depth of unevenness $\bar{d}$ =0.002 m which approximates the unevenness depths of experimental surfaces will be used for numerical simulations. Fig. 6 which presents the maximum displacement of the robot body versus $\bar{l}$ and v when k_s = 500 N/m, 1000 N/m, 1500 N/m and 2500 N/m can be applied to choose the optimal parameters $\bar{l}$, v and k_s to reduce the vibration of robot. For example, as can be seen from Figs. 6b and 6c, if the unevenness of ground $\bar{l}$ ranges from 0.05 m to 0.1 m and k_s ≤1000 N/m, the velocity should be higher than 0.4 m/s, when k_s ≥1000 N/m the velocity should be lower than 0.2 m/s to avoid the high vibration of robot.

In order to simulate the effectiveness of the absorber systems, let us choose parameters of the absorber systems and parameters of the OMR from the above investigations. For our purpose, the velocity of the robot ranges from 0.25 m/s to 0.5 m/s. Since the absorbers are designed to reduce the high-frequency disturbances so the length of unevenness $\bar{l}$ ≤ 0.1 m is applied for numerical simulations.

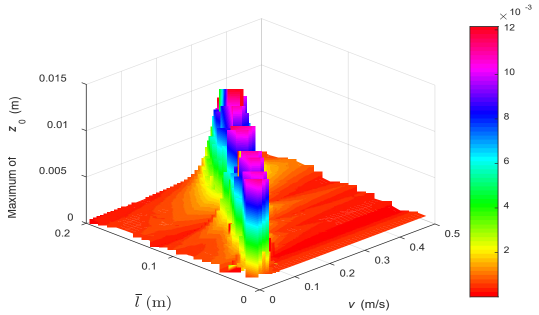

a) k_s = 500 N/m, $\bar{d}$ =0.001 m

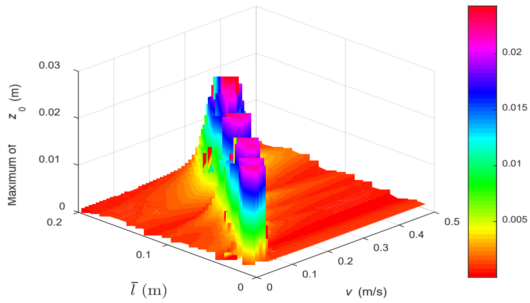

b) k_s = 500 N/m, $\bar{d}$ =0.002 m

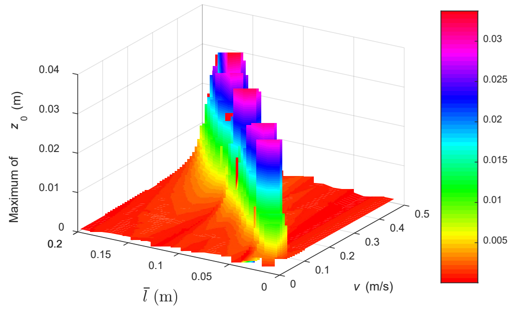

c) k_s = 1000 N/m, $\bar{d}$ =0.002 m

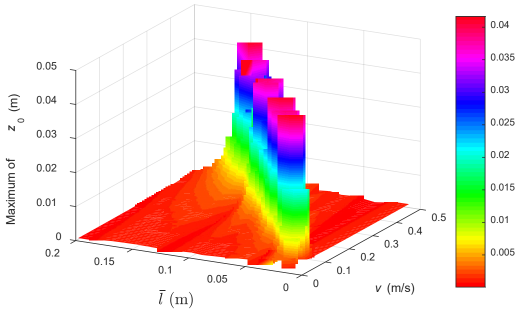

d) k_s = 1500 N/m, $\bar{d}$ =0.002 m

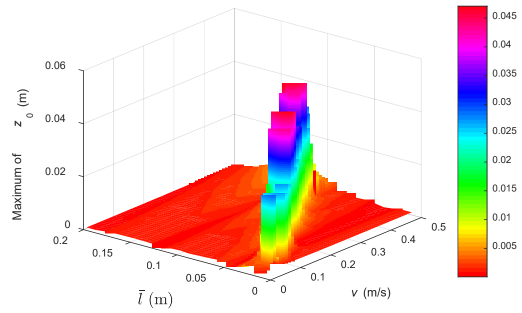

e) k_s = 2000 N/m, $\overline{d}$ =0.002 m

Fig. 6. Maximum displacement of the robot body versus $\overline{l}$ and v

With the selection of the velocity and the length of unevenness above, the spring constant and damping coefficient can be chosen as follows. From previous sections, when $k_s \leq 500$ N/m or $k_s \geq 1100$ N/m the damping coefficient c_s can be chosen arbitrary. Thus, for simplicity reason, c_s =0 is chosen. However, the spring should not be too low to avoid the large heave, rolling, and pitching of the robot so the spring constant k_s=1200 N/m is chosen for simulation. Finally, from the chosen ranges of the velocity and the length of unevenness, the velocity v=0.5 m/s and three different uneven grounds $\overline{l}$ =0.01m, 0.025m, 0.05m are applied for numerical simulations.

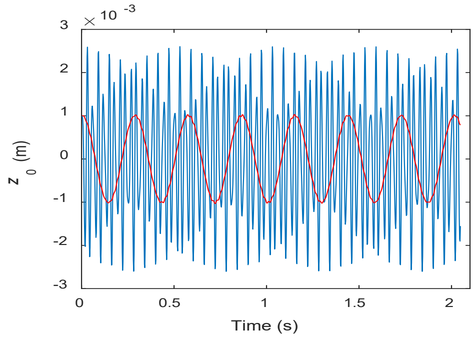

a) Displacement time history, $\overline{l}$ =0.01 m

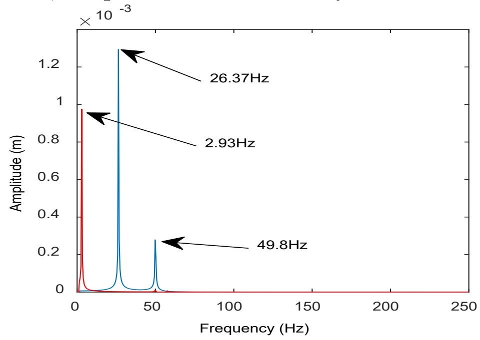

b) Frequency spectrum $\overline{l}$ =0.01 m

Figs. 7a, 7c, 7e present the displacements of the center of robot body for three cases $\overline{l}$ =0.01 m, $\overline{l}$ =0.025 m, and $\overline{l}$ =0.05 m. As can be seen from this figure, when $\overline{l}$ =0.01 m, the vibration of robot body reduces about 60%. When $\overline{l}$ =0.025 m, the vibration of robot body reduces about 60%. When $\overline{l}$ increase to 0.025 and up to 0.05 m, the vibration of robot body reduces about 75%. These results show the efficiency of the chosen parameters of the OMR to reduce its vibration when it moves on uneven surfaces.

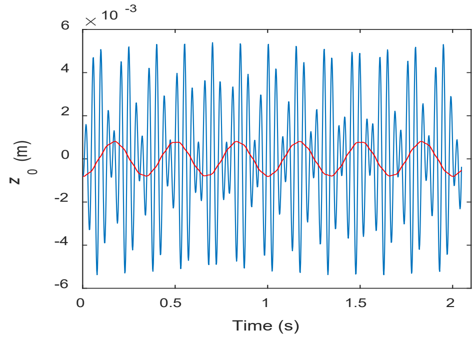

c) Displacement time history, $\overline{l}$ =0.025 m

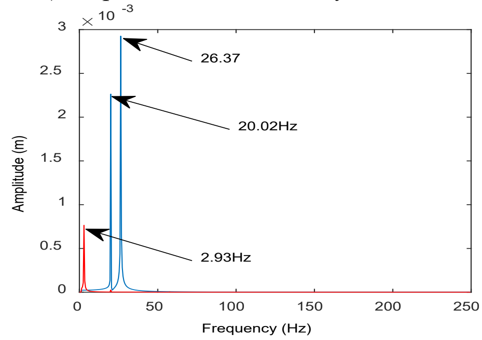

d) Frequency spectrum $\overline{l}$ =0.025 m

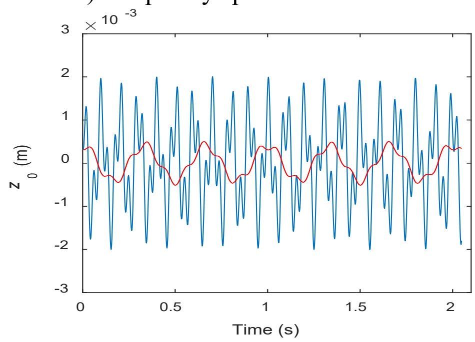

e) Displacement time history, $\overline{l}$ =0.05 m

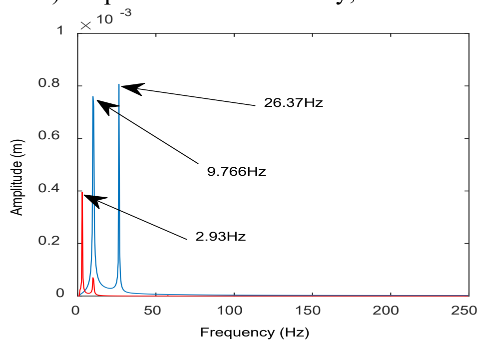

f) Frequency spectrum $\overline{l}$ =0.05 m

Fig. 7. Displacement of robot body: Blue line: k_s=2.0x10^{11} N/m; Red line: k_s=1200 N/m

Figs. 7b, 7d, 7f present the corresponding frequency spectrums for three different unevenness surfaces. As can be seen from these figures, when the OMR without absorbers moves on different uneven surfaces, high-frequency disturbances occur at 20.02 Hz, 26.37 Hz, 49.8 Hz. However, when the absorbers are applied, these high-frequency disturbances are filtered out and the OMR vibrates at low frequency of 2.93 Hz which will be helpful for the purpose of image-base mobile robot.

Experimental results

The OMR was manufactured and applied for the test as depicted in Fig. 8. Three omnidirectional wheels are applied for the OMR. The robot consists of the upper part with masses of 10 kg and the lower part including three wheels with masses of 2.5 kg. Thus, each wheel mass can be considered as 2.5/3 kg. Three absorbers consisting of two springs with equivalent spring constant of 1200 N/m are applied. The velocity of robot is 0.5m/s. The vibration of robot was measured by using the B&K accelerometer and Pulse instrument. The accelerometer was installed on the robot body. In our experiments, three scenarios for uneven ground to investigate the efficiency of the design of OMR are presented in Table 1.

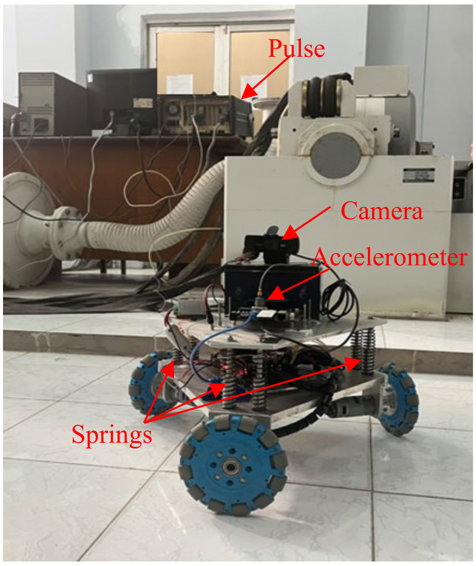

a)

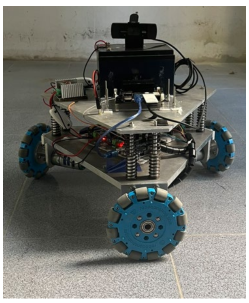

b)

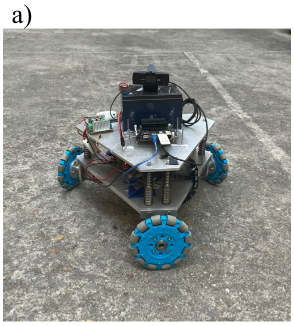

c)

Fig. 8. The OMR in the experiment: a) Scenario 1; b) Scenario 2; c) Scenario 3

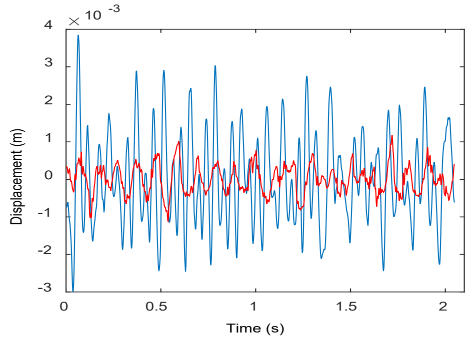

a) Displacement time history

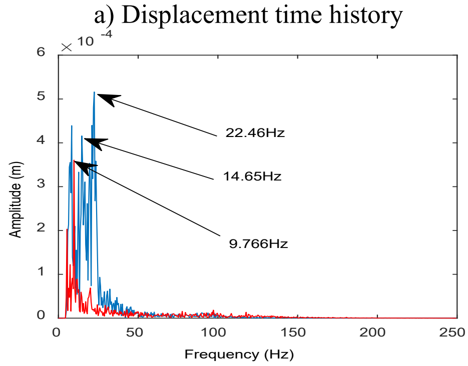

b) Frequency spectrum

Fig. 9. Displacement of robot body on the 1st ground: Blue line: k_s=2.0x10^{11} N/m; Red line: k_s=1200 N/m

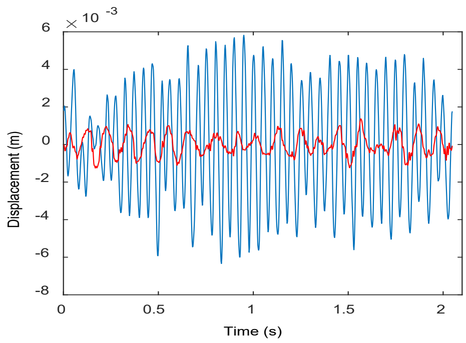

a) Displacement time history

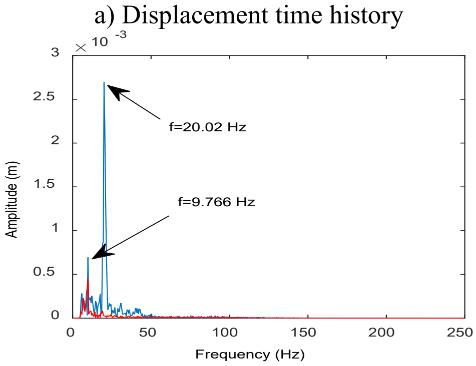

b) Frequency spectrum

Fig. 10. Displacement of robot body on the 2nd ground: Blue line: k_s=2.0x10^{11} N/m; Red line: k_s=1200 N/m

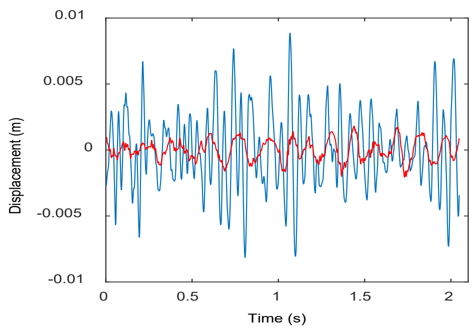

a) Displacement time history

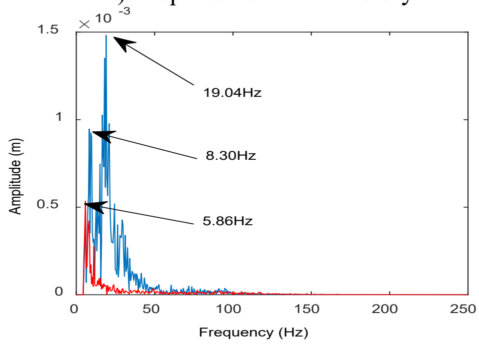

b) Frequency spectrum

Fig. 11. Displacement of robot body on the 3rd ground: Blue line: k_s=2.0x10^{11} N/m; Red line: k_s=1200 N/m

Table 1. Three scenarios for unevenness ground

Scenario	Type of ground
1	Floral tiled floor
2	Normal tiled floor
3	Concrete floor

Figs. 9a, 10a and 11a present the comparison of vibrations of the robot body without and with the designed absorbers in the three scenarios. For the first scenario, when the ground is smoothest, the vibration amplitude of the robot without absorbers is around 3 mm and it reduces to 1 mm when the absorbers are applied. This means that the vibration of robot with absorbers reduces about 67% in comparison with the robot without absorbers. For the second scenario, the unevenness of ground increases, the vibration of the robot without absorbers increases to about 6 mm. When absorbers are applied, the vibration amplitude of the robot reduces significantly to 1mm which corresponds to the vibration reduction of about 83%. For the third scenario, when the ground is roughest, the maximum vibration amplitude of the robot without absorbers is about 8 mm. When absorbers are applied, the vibration amplitude of the robot reduces to 2 mm which corresponds to the vibration reduction of about 75%. These results verify the efficiency of the proposed method for the vibration reduction of the OMR to improve the quality of the images captured from the mobile robot.

Figs. 9b, 10b and 11b present the frequency spectrums for three different surfaces. As can be seen from these figures, when the absorbers are applied, high frequencies at 14.65 Hz, 20.02 Hz and 22.46 Hz are filtered out. The OMR vibrates at lower amplitudes and at lower frequencies of 5.86 Hz and 9.766 Hz. These experimental results are in agreement with the simulation results justifying the efficiency of the method for removing high-frequency disturbances and reducing the vibration amplitude of the OMR.

Conclusions

This paper presents the theoretical background for the optimal design of an OMR to reduce the vibration when it moves on uneven grounds. In this paper, the derivation of the governing equations of motion of the OMR moving on uneven grounds is obtained.

The proposed equations are applied to simulate the relationship between the parameters of the robot and the vibration amplitude in order to choose the optimal parameters for the purpose of reducing the vibration of robot.

The numerical simulations from chosen parameters of the robot show that the vibration of the robot equipped with absorber systems can reduce up to about 75 % in comparison with the robot without absorber systems. Moreover, when the absorbers are applied, the high-frequency disturbances causing by the unevenness of grounds are filtered out and the OMR vibrates at a low frequency. These simulation results show the effectiveness of the proposed method.

The experiment has been caried out to verify the proposed design of the OMR. Very good agreement between simulation results and experimental results verifies the efficiency of the proposed method for reducing the vibration of the OMR moving on uneven grounds which will be helpful to improve the quality of images captured from the mobile robot.

Acknowledgements

This research is funded by the Vietnam Academy of Science and Technology under grant number VAST 01.01/21-22.

Declaration of interests

The authors declare that they have no known competing financial interests or personal relationships that could have appeared to influence the work reported in this paper.

References

Alan W. A.J Piergiovanni, Michael S.R., "Model-based behavioral cloning with future image similarity learning". 3rd Annual Conference On Robot Learning, CoRL 2019, Osaka, Japan, Proceedings.

Ashish K., Saurabh G., David F., Sergey L., Jitendra M., "Visual memory for robust path following". Advances In Neural Information Processing Systems, Vol. 31, 2018, pp. 765–774.

Baede T.A., Motion control of an omnidirectional mobile robot. Traineeship report DCT 2006.

Campion G., Bastin G. and D'Andréa-Novel B., "Structural Properties and Classification of

Kinematic and Dynamic Models of Wheeled Mobile Robots". IEEE Transactions on Robotics and Automation, Vol. 12, No. 1, pp.47-62, 1996.

Charfeddine M., Sakiichi O., Yoshitsugu K., Hiroaki S., "Vibration control of mobile robot vehicle by dynamic vibration absorber". JSME International Journal, 42 (1), 1999.

Chelsea F., Ian G., Sergey L., "Unsupervised learning for physical interaction through video prediction". Advances In Neural Information Processing Systems, Vol. 29, 2016, pp. 64–72.

Cheng C.W., Yong Q.Z., "Identification and Machine Learning Prediction of Nonlinear Behavior in a Robotic Arm System". Symmetry-Basel, Vol. 13(8), 2021, pp.1445–1471.

Chih-Jer L., Hsing-Cheng W. and Cheng-Chi W., "Automatic calibration of Tool Center Point for six degree of freedom robot". Actuators, Vol. 12(3), 2023, 107.

Christian P.C., Andreas P., Martin H., Verl A., "Control of an Pseudo-Omnidirectional, Non-Holonomic, Mobile Robot based on an ICM Representation in Spherical Coordinates", Proceedings of the 47th IEEE conference on Decision and Control, pp. 4976-4983, 2008.

Davood N., Ali M. and Durali M., "Dynamic modeling and analysis of a two d.o.f. mobile manipulator". Robotica 19, 2001, 177–185.

Deepak P., Parsa M., Guanghao L., Pulkit A., Dian C., Yide S., Evan S., Jitendra M., Alexei A.E., Trevor D., "Zero-shot visual imitation". ICLR, 2018.

Ebert F., Chelsea Finn., Alex X.L., Sergey L., "Self-supervised visual planning with temporal skip connections". Proceedings Of The 1st Annual Conference On Robot Learning, Vol. 78, 2017, pp. 344–356.

Felix J.L.P., Silva E.L., Balthazar J.M., Tusset, A. M., Bueno, A. M., Brasil, R.M.L.R.F., "On nonlinear dynamics and control of a robotic arm with chaos". Proceedings of the 2014 International Conference On Structural Nonlinear Dynamics And Diagnosis, Agadir, Morocco, 2014; Volume 16, 1–6.

Guoliang Z., Yukinori K., Takanori E. and Yohei H., "Approaches based on particle swarm optimization for problems of vibration reduction of suspended mobile robot with a manipulator". Journal of Vibration and Control 20(1), 2012, 3-23.

Hamid T., Chun X., "Omnidirectional mobile robots, mechanisms and navigation approaches". Mechanism and Machine Theory 153 (2020) 103958.

Liu H., Nonami K., Hagiwara T., "Semi-active fuzzy sliding mode control of full vehicle and suspensions". Journal of Vibration and Control, 11(8), 2005, 1025–1042.

Mark A. and Nick B., "Omni-drive Robot Motion on Curved Paths: The Fastest Path between Two Points Is Not a Straight-Line". AI 2002: Advances in Artificial Intelligence, vol. 2557, 2002, pp. 225-236.

Masao N., "Resent researches on active suspensions for ground vehicles". Int. J. JSME, Ser. C, Vol. 36 (2), 1993, 161-170.

Matsuhisa H., Roug R., Jing W.Y., Nishihara O., Sato S., "Vibration control of a rope wave carrier by passive dynamic vibration absorbers". Int. J. JSME, Ser. C, Vol. 38(4), 1995, 657-661.

Noriaki H., Amir S., Fei X., Roberto M.M., Silvio S., "VUNet: Dynamic scene view synthesis for traversability estimation using an RGB camera". IEEE Robot. Autom. Lett. 4 (2) (2019) 2062–2069, http://dx.doi. org/10.1109/LRA.2019.2894869.

Noriaki H., Fei X., Roberto M.M., Amir S., Silvio S., "Deep visual MPC-policy learning for navigation". IEEE Robot. Autom. Lett. 4 (4) (2019) 3184–3191.

Patrick F., William H.W., Andrew D., and Michael J.T., "Do Humans Integrate Routes Into a Cognitive Map? Map- Versus Landmark-Based Navigation of Novel Shortcuts". Journal of Experimental Psychology: Learning, Memory, and Cognition 2005, Vol. 31, No. 2, 195–215.

Patrick F.M., Charies N., Kinematic Modeling of Wheeled Mobile Robots. Technical Report, Carnegie-Mellon University, Pittsburgh, Pennsylvania, pp. 10-13, 1986.

Pouria R., Ehab A.K., Yildirim H., "Nonlinear dynamics and control of an inertially actuated jumper robot". Nonlinear Dyn. (2019), 97, 161–176.

Rainer B., "HERMES - A Humanoid Mobile manipulator for service Tasks". Proceedings of the FSR'97 Conference on Field and Service Robots, pp. 508-515, 1997.

Reza N.J., Vehicle dynamics theory and application. Springer, New York, 2008.

Sangdae K., Seungwo K., "A Development of 3-Wheels Omni-Directional Mobile Robot Using Fuzzy Logic". SCIS & ISIS 2010, Okayama Convention Center, Okayama, Japan.

Yong L., Xiaofei W., J. Jim Zhu; Jae L., "Omni-directional mobile robot controller design by trajectory linearization". Proceedings of the American Control Conference, vol. 4, 2003, pp. 3423-3428.

Youngkak M., Seungwoo K., "A Study on Development of Home Mess-Cleanup Robot McBot". Proceedings of the 2008 IEEE/ASME International Conference on Advanced Intelligent Mechatronics, pp.114-119.

Yu I. and Masaki T., "Empirical study of future image prediction for image-based mobile robot navigation". Robotics and Autonomous Systems 150 (2022) 104018.